catalysts

MDPI

Communication

# The Fabrication of $Ga_2O_3$/ZSM-5 Hollow Fibers for Efficient Catalytic Conversion of *n*-Butane into Light Olefins and Aromatics

**Jing Han, Guiyuan Jiang *, Shanlei Han, Jia Liu, Yaoyuan Zhang, Yeming Liu, Ruipu Wang, Zhen Zhao *, Chunming Xu, Yajun Wang, Aijun Duan, Jian Liu and Yuechang Wei**

Received: 7 November 2015; Accepted: 29 December 2015; Published: 15 January 2016
Academic Editor: Andreas Martin

State Key Laboratory of Heavy Oil Processing, China University of Petroleum, Beijing 102249, China; hanjinglucky@163.com (J.H.); hanshanlei891024@163.com (S.H.); liujcup@126.com (J.L.); zyy291495935@163.com (Y.Z.); liuym128@163.com (Y.L.); wrpkeepup@163.com (R.W.); xcm@cup.edu.cn (C.X.); wangyajun@cup.edu.cn (Y.W.); duanaijun@cup.edu.cn (A.D.); liujian@cup.edu.cn (J.L.); weiyc@cup.edu.cn (Y.W.)

* Correspondence: jianggy@cup.edu.cn (G.J.); zhenzhao@cup.edu.cn (Z.Z.); Tel.: +86-10-8973-9125 (G.J.); +86-10-8973-1586 (Z.Z.)

**Abstract:** In this study, the dehydrogenation component of $Ga_2O_3$ was introduced into ZSM-5 nanocrystals to prepare $Ga_2O_3$/ZSM-5 hollow fiber-based bifunctional catalysts. The physicochemical features of as-prepared catalysts were characterized by means of XRD, BET, SEM, STEM, $NH_3$-TPD, *etc.*, and their performances for the catalytic conversion of *n*-butane to produce light olefins and aromatics were investigated. The results indicated that a very small amount of gallium can cause a marked enhancement in the catalytic activity of ZSM-5 because of the synergistic effect of the dehydrogenation and aromatization properties of $Ga_2O_3$ and the cracking function of ZSM-5. Compared with $Ga_2O_3$/ZSM-5 nanoparticles, the unique hierarchical macro-meso-microporosity of the as-prepared hollow fibers can effectively enlarge the bifunctionality by enhancing the accessibility of active sites and the diffusion. Consequently, $Ga_2O_3$/ZSM-5 hollow fibers show excellent catalytic conversion of *n*-butane, with the highest yield of light olefins plus aromatics at 600 °C by 87.6%, which is 56.3%, 24.6%, and 13.3% higher than that of ZSM-5, ZSM-5 zeolite fibers, and $Ga_2O_3$/ZSM-5, respectively.

**Keywords:** *n*-butane; catalytic conversion; bifunctional catalyst; ZSM-5 hollow fiber; $Ga_2O_3$

## 1. Introduction

Light olefins, including ethene, propene, butene, *etc.* are important basic chemical raw materials and the demand for them stays at a high level. Aromatic hydrocarbons, such as benzene, toluene, and xylene, are also significant materials for organic chemical production, which are widely used in the production of synthetic fiber, resin, and rubber. For the past few years, crude processing capacity of refinery continues to improve, resulting in the by-production of a large amount of C4 hydrocarbons. Among C4 hydrocarbons, many processes on the conversion of C4 alkenes have been reported, including catalytic cracking, disproportionation, *etc.* However, C4 alkanes, as important components of C4 hydrocarbons, due to their high stability, the chemical utilization efficiency is still low. Currently, they are mostly used as low-added value fuel. So, using less valuable but industrially abundant C4 alkanes as feedstock to produce light olefins and aromatics has been attracting increasing attention [1–3].

Compared with the current main process of steam cracking for the production of light olefins, catalytic cracking, due to the introduction of catalyst, can reduce the reaction temperature and energy

consumption, and it also can improve the selectivity to light olefins, especially to that of propylene [4]. Up to now, three kinds of catalysts have been proposed for catalytic cracking of hydrocarbons, including zeolites [5–7], metal oxides [8,9], and composite catalysts [10,11]. Among various catalysts, ZSM-5 zeolite is a typical and superior candidate because of its excellent stability, adjustable acidity, and special pore structure [3,12–14]. To further improve the catalytic cracking performances of ZSM-5 zeolite, many modifications have been reported, including alkaline earth metal [15], transition metal [16], rare earth elements [17], phosphorus modification, *etc*. [18]. The above modifications can modulate the amount of acidic sites and the acid strength of ZSM-5 zeolites, thus enhancing the selectivity to light olefins and promoting the catalytic performances of ZSM-5.

In addition to the regulation of acidity, the optimization of the pore structure is another effective strategy to enhance the catalytic performances of zeolite catalysts. In this context, nano ZSM-5 zeolites [19], mesoporous ZSM-5 zeolites [20], nanosheets of zeolite [21], and other hierarchical ZSM-5 zeolites [12] have been reported. Due to the introduction of pores with different levels, the accessibility of active sites of hierarchical ZSM-5 zeolites can be improved greatly. Meanwhile, the transportation capability for feedstock of large sizes could be also enhanced. Among various hierarchical ZSM-5 zeolites, hierarchical ZSM-5 fibers have received much concern because the hierarchical ZSM-5 fibers not only possess the high catalytic activity of zeolite, but also have high mass transfer performance and low pressure drop. Previously, we reported a versatile and facile method for the fabrication of hierarchical ZSM-5 zeolite fibers with macro-meso-microporosity by coaxial electrospinning, and it was found that suitable acidity and the hierarchical porosity contribute to the excellent catalytic performances in the catalytic cracking of *iso*-butane [12].

Although many catalysts have been proposed for catalytic cracking of C4 alkanes, there are few reports on the catalysts for efficient conversion of *n*-butane, the most stable component in C4 hydrocarbons. To promote the catalytic conversion of *n*-butane, the introduction of dehydrogenation component in the current acid-based zeolite to construct the bifunctional catalyst may provide a good solution [22,23]. Many metal oxide-based catalysts have been reported for the dehydrogenation of alkanes, such as vanadia-based [24,25], chromium-based [26–28], gallium-based [29,30], *etc.* So in the present study, using *n*-butane as feedstock, we chose $Ga_2O_3$ as the dehydrogenation component and introduced it into the ZSM-5 nanocrystals to fabricate $Ga_2O_3$/ZSM-5 hollow fiber based bifunctional catalysts. The physicochemical features of as-prepared catalysts were characterized by means of XRD, BET, SEM, STEM, $NH_3$-TPD, *etc.*, and their performance for the catalytic conversion of *n*-butane to produce light olefins and aromatics were investigated.

## 2. Results and Discussion

### *2.1. Catalyst Characterization*

Figure 1 shows the XRD patterns of the as-synthesized catalysts. From Figure 1 the characteristic diffraction peaks of ZSM-5 could be seen, showing that the catalysts are typical of MFI topology and the introduction of gallium on ZSM-5 does not change the crystalline structure of ZSM-5. No obvious diffraction peaks corresponding to gallium species are observed in the XRD patterns of Ga/ZSM-5, indicating that gallium species may be well dispersed on the surface of ZSM-5 zeolite [31] or the amount of them is too low to show obvious diffraction peak. According to the Ga $2p_{3/2}$ XPS spectra (Figure 2), the Ga $2p_{3/2}$ binding energy value (BEs) for the as-prepared Ga/ZSM-5 (1118.3 eV) is consistent with that for $Ga_2O_3$, indicating that the gallium exists on the surface of ZSM-5 in the form of $Ga_2O_3$. In comparison with that of the single bulk $Ga_2O_3$, the broadening of the half peak width of Ga $2p_{3/2}$ of the as-prepared $Ga_2O_3$/ZSM-5 occurs, which is connected with the increase of the Ga dispersion [32].

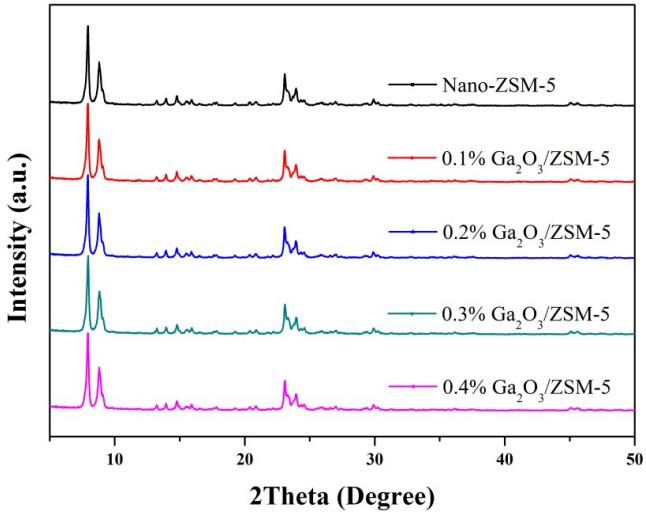


**Figure 1.** XRD patterns of the as-synthesized $Ga_2O_3$/ZSM-5 and Nano-ZSM-5.

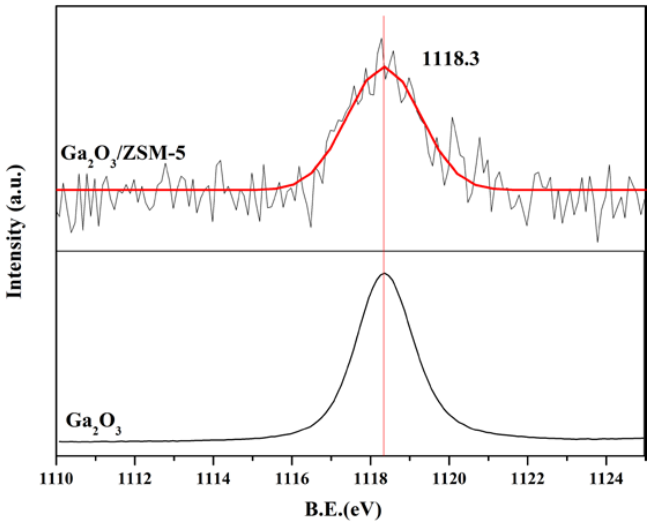


**Figure 2.** Ga $2p_{3/2}$ XPS spectra of $Ga_2O_3$ and $Ga_2O_3$/ZSM-5.

Figure 3A shows the SEM image of the synthesized Nano-ZSM-5 with the average particle size of 137 nm. After the introduction of $Ga_2O_3$ on Nano-ZSM-5 by impregnation (Figure 3B), the morphology and particle size of $Ga_2O_3$/ZSM-5 do not show obvious change. Then, $Ga_2O_3$/ZSM-5 was used as building blocks for the preparation of $Ga_2O_3$/ZSM-5 hollow fibers via coaxial electrospinning. Specifically, a suspension of $Ga_2O_3$/ZSM-5 nanocrystals in polyvinylpyrrolidon (PVP)/ethanol solution used as the outer fluid, and paraffin oil acted as the inner liquid. The addition of PVP in the suspension was to provide appropriate viscosity for the fluent electrospinning, and paraffin oil, the inner liquid, was to present hollow structure via calcination. The $Ga_2O_3$/ZSM-5/PVP composite fibers were successfully prepared (Figure 3C), and after temperature-programmed calcination, the PVP and paraffin oil were removed, and hierarchical $Ga_2O_3$/ZSM-5 hollow fibers were obtained (Figure 3D). From Figure 3D, hollow structure and comparatively uniform diameter of the as-prepared fibers could be well seen. Figure 3E presents the high magnification SEM image of the red square in Figure 3D, and it clearly shows that the wall of the $Ga_2O_3$/ZSM-5 zeolite hollow fibers is composed of $Ga_2O_3$/ZSM-5 nanoparticles, with uniform macropores on the hollow fiber level. The TEM image (Figure 3F) of the fibers further proves the continuous hollow structure character of the fibers. The EDAX elemental

maps present the element distribution of Si, O, Al, and Ga (Figure 4), and bright green dots indicates that Ga element is well dispersed on the as-prepared $Ga_2O_3$/ZSM-5 hollow fibers.

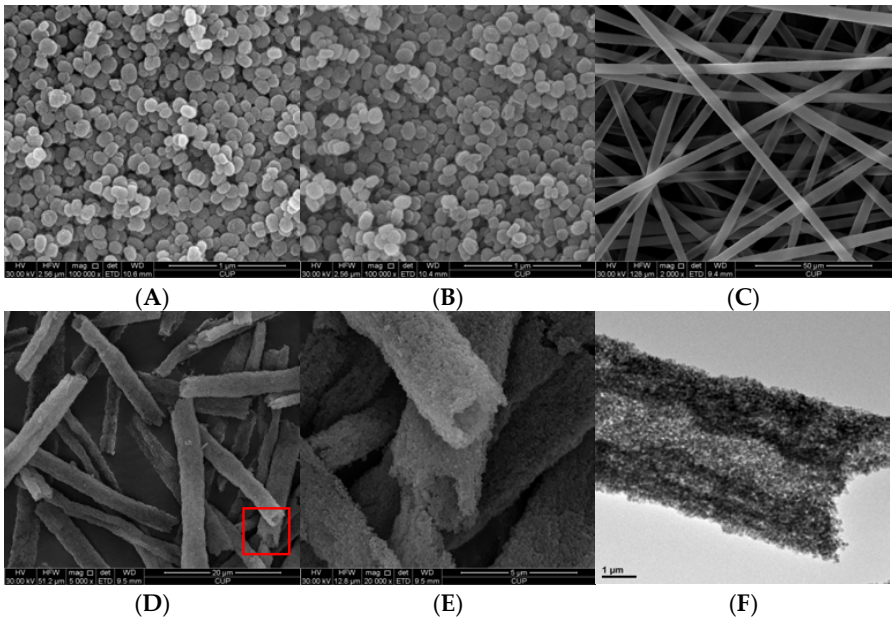


**Figure 3.** SEM images of the as-prepared Nano-ZSM-5 (**A**); 0.3% $Ga_2O_3$/ZSM-5 (**B**); 0.3% $Ga_2O_3$/ZSM-5/PVP fibers before calcination (**C**); the low (**D**) and magnified (**E**) SEM images of 0.3% $Ga_2O_3$/ZSM-5 hollow fibers after calcination at 550 °C, respectively; TEM image (**F**) of one hollow fiber after calcination at 550 °C.

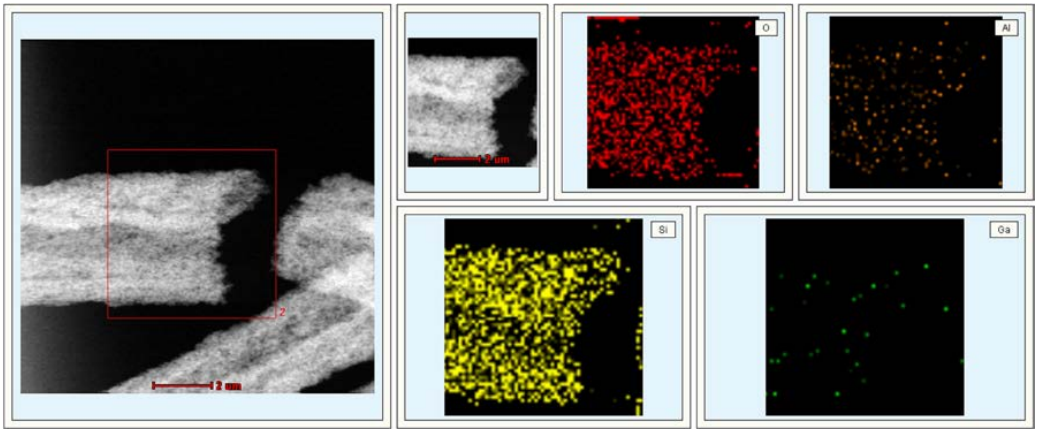


**Figure 4.** EDAX elemental maps of Si, O, Al, and Ga of 0.3% $Ga_2O_3$/ZSM-5 zeolite hollow fibers.

Figure 5 shows the nitrogen adsorption-desorption isotherms and BJH pore size distribution (inset) of the $Ga_2O_3$/ZSM-5 hollow fibers. According to the nitrogen adsorption-desorption measurement, the Brunauer-Emmett-Teller (BET) surface area of 377 $m^2/g$ and the pore volume of 0.275 $cm^3/g$ were determined. From Figure 5, it can be seen that the present isotherms exhibit a typical hysteresis loop at $p/p_0 > 0.1$, indicating mesopores are formed, arising from the interparticle voids of $Ga_2O_3$/ZSM-5. Hence, the as-prepared $Ga_2O_3$/ZSM-5 hollow fibers exhibit a good hierarchical macro-meso-microporosity, with micropores in ZSM-5 nanoparticles, mesopores formed by the stacking of the $Ga_2O_3$/ZSM-5 nanoparticles, and continuous macropores on the hollow fibers.

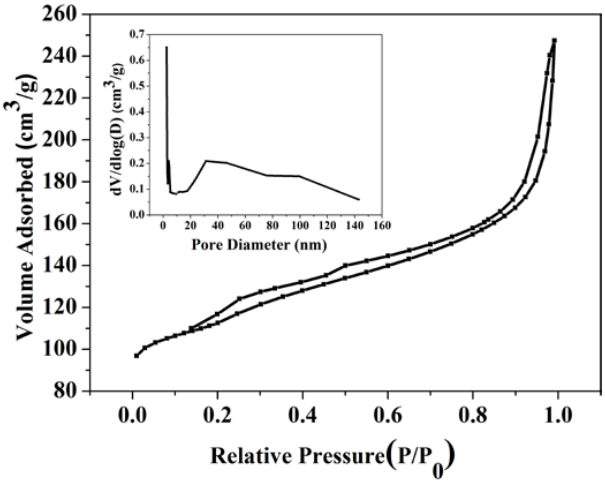


**Figure 5.** Nitrogen adsorption-desorption isotherms and BJH pore size distribution (inset) of the 0.3% $Ga_2O_3$/ZSM-5 zeolite hollow fibers.

The temperature-programmed desorption of ammonia ($NH_3$-TPD) experiments were conducted to obtain the acidic properties of the as-prepared $Ga_2O_3$/ZSM-5. Figure 6 presents $NH_3$-TPD profiles of $Ga_2O_3$/ZSM-5. From Figure 6, it can be seen that there are two desorption group peaks for ZSM-5, one is in the range of 150–250 °C, corresponding to the weak acid sites, and the other, *i.e.*, the strong acid sites, reside in the range of 300–450 °C. After the introduction of $Ga_2O_3$, there is no shift of the diffraction peaks, indicating that the strength of acidic sites does not change. Among the samples, except 0.2% $Ga_2O_3$/ZSM-5, the amount of weak acid does not show apparent change, and only the amount of strong acid shows a slight decrease (Table S1).

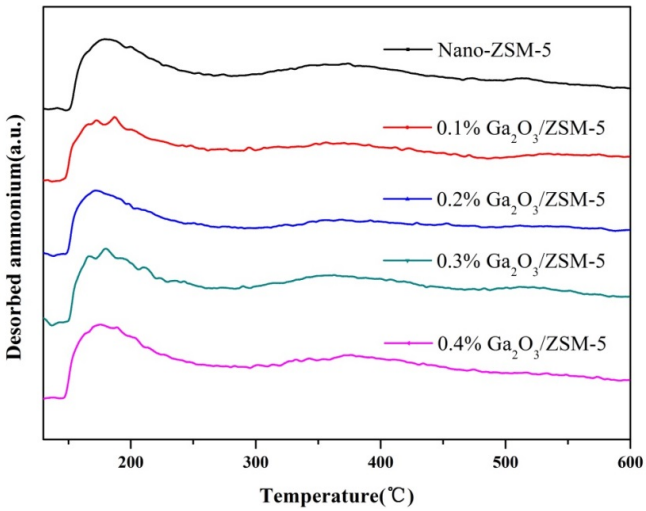


**Figure 6.** $NH_3$-TPD profiles of $x$% $Ga_2O_3$/ZSM-5($x$ = 0, 0.1, 0.2, 0.3, 0.4).

## 2.2. Catalytic Preformances

Before investigating the catalytic performance of $Ga_2O_3$/ZSM-5 hollow fibers, to check whether an optimal introducing of $Ga_2O_3$ on ZSM-5 exists, $Ga_2O_3$/ZSM-5 catalysts with different $Ga_2O_3$ loading were evaluated. Figure 7 shows the conversion of *n*-butane (A), yield of ethene and propene (B), and yield of $C_2^=$, $C_3^=$, $C_4^=$ plus BTX ($C_2^=$, $C_3^=$, $C_4^=$ plus BTX refer to ethene, propene, butenes, butadiene and benzene, toluene, xylene) (C) as a function of reaction temperature. From Figure 7, it is apparent that with increase of the reaction temperature, the conversion of *n*-butane, the yield of ethene

and propene and the yield of $C_2^=$, $C_3^=$, $C_4^=$ plus BTX on all catalysts markedly increase. And at the same temperatrue, increasing the $Ga_2O_3$ loading results in the increase of the conversion and the yield of $C_2^=$, $C_3^=$, $C_4^=$ plus BTX. As for the yield of ethene and propene, when the reaction temperature is lower than 600 °C, it increases with the increasing loading of $Ga_2O_3$, while when the temperature is above 625 °C, the yield of ethene and propene decreases with increasing the loading of $Ga_2O_3$. Such a result could be attributed to the synergistic effect of the dehydrogenation and aromatization properties of $Ga_2O_3$ [33] and the cracking function of ZSM-5. At lower temperatures, due to the dehydrogenation property, the presence of $Ga_2O_3$ contributes to the activation and dehydrogenation of *n*-butane. Hence *n*-butane may undergo dehydrogenation to produce butene, which is much easier to be converted than *n*-butane, and then, butene will undergo catalytic cracking reaction to produce ethene and propene as primary products. When temperature is above 625 °C, the produced ethene and propene will undergo oligomerization to produce higher olefins (C2–C9), and then, C7–C9 alkylcyclohexenes would be formed by cyclization and dehydrogenation. Finally, C7–C9 alkylcyclohexenes are converted to corresponding aromatics [34]. Thus, although the increase of the yield of ethene and propene flattens out with the increase of the temperature, the generation of the benzene, toluene, and xylene results in the yield of $C_2^=$, $C_3^=$, $C_4^=$ plus BTX continuing to increase. From Figure 7, it is can be seen that when the $Ga_2O_3$ loading amount is above 0.3%, the enhancing capacity of the conversion of *n*-butane and the yield of $C_2^=$, $C_3^=$, $C_4^=$ plus BTX is not obvious. According to the literature [35], one possible explanation is that a very small amount of gallium is sufficient to cause a marked enhancement in the activity of ZSM-5, and too much gallium loading will lead to excessive dehydrogenation and secondary reaction, resulting in no beneficial improvement in catalytic conversion of *n*-butane. In addition, according to the $NH_3$-TPD results (Figure 6), the introduction of $Ga_2O_3$ slightly decreased the amount of strong acid of ZSM-5, so with the increase of the $Ga_2O_3$ loading, the decreased acidity property results in the decrease of cracking performance. The present result indicates that excellent catalytic activity could be obtained by regulating of the $Ga_2O_3$, leading to a good balance between the dehydrogenation of $Ga_2O_3$ and the cracking function of ZSM-5. Given that 0.3% $Ga_2O_3$/ZSM-5 was chosen as building blocks for the preparation of $Ga_2O_3$/ZSM-5 hollow fibers via coaxial electrospinning, and their catalytic conversion of *n*-butane into light olefins and aromatics was further investigated.

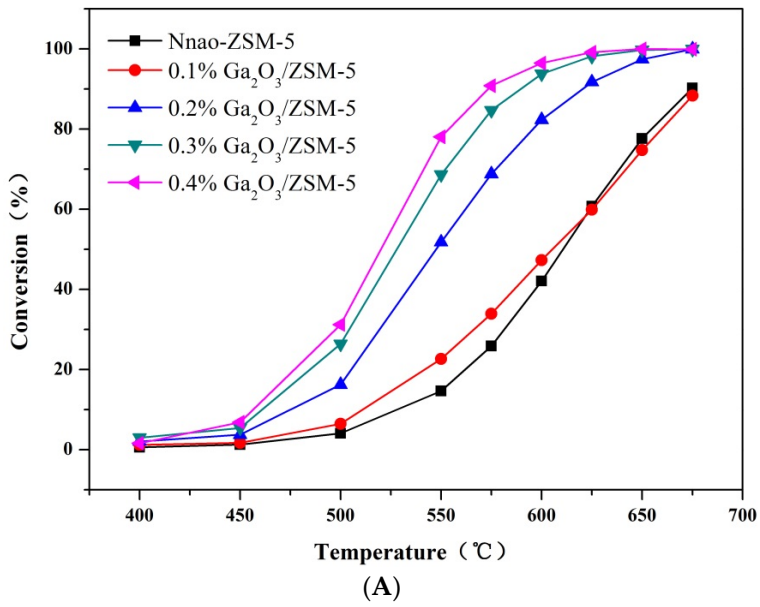


**Figure 7.** *Cont.*

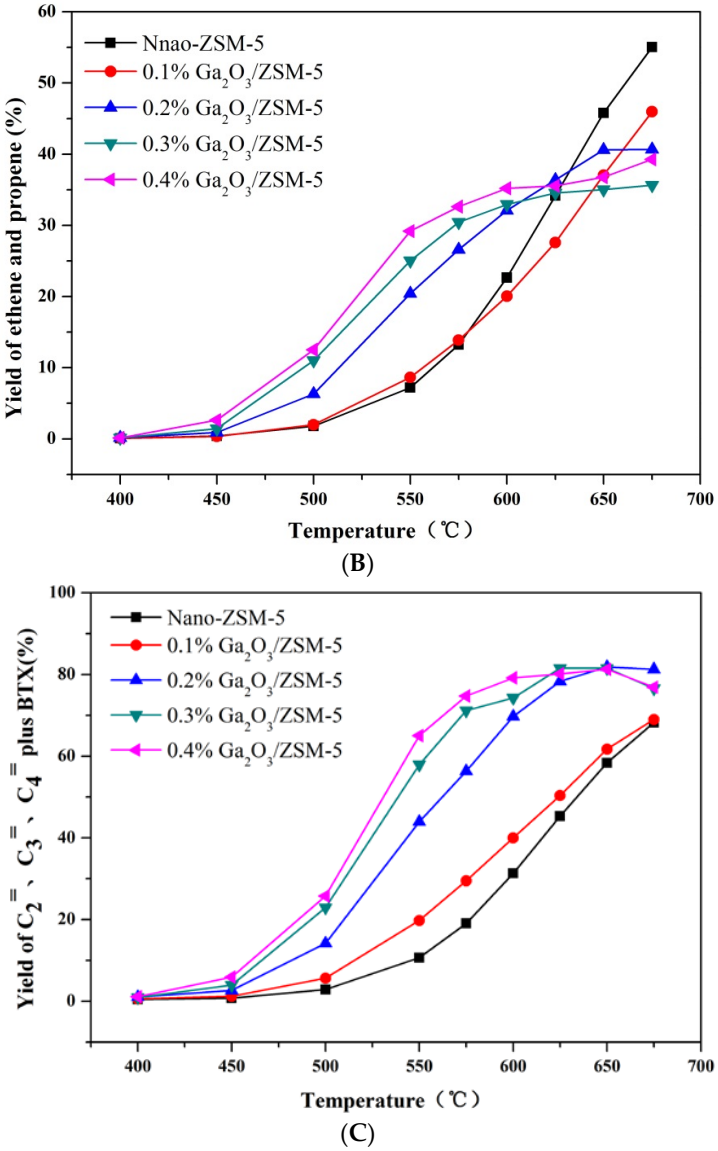


**Figure 7.** The conversion of *n*-butane (**A**); the yield of ethane and propene (**B**) and $C_2^=$, $C_3^=$, $C_4^=$ plus BTX (**C**) of the catalysts with different $Ga_2O_3$ loadings as a function of reaction temperatures.

Figure 8 shows the conversion of *n*-butane (A) and the yield of $C_2^=$, $C_3^=$, $C_4^=$ plus BTX (B) on the as-prepared 0.3% $Ga_2O_3$/ZSM-5 hollow fibers. For comparison, the catalytic performance of Nano-ZSM-5, 0.3% $Ga_2O_3$/ZSM-5 nanoparticles and the hierarchical ZSM-5 hollow fibers electrospun by the as-prepared Nano-ZSM-5 were also investigated. From Figure 8, it can be seen that with increasing the reaction temperature, the conversion of *n*-butane increases on all catalysts. Among the four catalysts, $Ga_2O_3$/ZSM-5 hollow fibers exihits the best catalytic reactivity in the whole temperature range. At the temperature of 575 °C the conversion of *n*-butane is almost 100%. Similar phenomenon is also reflected in the yield of $C_2^=$, $C_3^=$, $C_4^=$ plus BTX. When the reaction temperatures are lower than 650 °C, the yield of $C_2^=$, $C_3^=$, $C_4^=$ plus BTX on the four catalysts follows the order of $Ga_2O_3$/ZSM-5 hollow fibers > $Ga_2O_3$/ZSM-5 > ZSM-5 hollow fibers > Nano-ZSM-5. According to the catalytic behavior of four catalysts, specifically, compared with Nano-ZSM-5 and ZSM-5 hollow fibers, the catalytic performances of $Ga_2O_3$/ZSM-5 and $Ga_2O_3$/ZSM-5 hollow fibers are enhanced, respectively, indicating that the introduction of $Ga_2O_3$ is beneficial to the dehydrogenation of *n*-butane and thus promotes the catalytic activity of the catalysts efficiently. Meanwhile, in comparison with

the present Nano-ZSM-5 and $Ga_2O_3$/ZSM-5 as well as magnesium-containing HZSM-5 reported in the literature [15], the catalytic reactivities of hollow fibers of both ZSM-5 and $Ga_2O_3$/ZSM-5 are improved, indicating that the hierarchical pore structure of hollow fibers contributes to enhancing the whole catalytic performance. There exists a synergistic effect between $Ga_2O_3$/ZSM-5 (or ZSM-5) and the hierarchical porosity of the hollow fibers. The unique hierarchical macro-meso-microporosity structure of the as-prepared hollow fibers can effectively enhance the accessibility of the feedstock to catalytic active sites and facilitates the mass transfer of targeted products, including ethene, propylene, aromatics, *etc.* Thus, the secondary reactions of ethene and propene as well as the carbon deposition could be hindered [12]. $Ga_2O_3$/ZSM-5 hollow fibers, which effectively combine the cracking function of ZSM-5, the hierarchical macro-meso-microporosity of hollow fibers, and the dehydrogenation of $Ga_2O_3$, show the best catalytic behavior among the four catalysts, with the highest yield of $C_2^=$, $C_3^=$, $C_4^=$ plus BTX at 600 °C by 87.6%, which is 56.3%, 24.6%, and 13.3% higher than ZSM-5, ZSM-5 zeolite fibers, and 0.3% $Ga_2O_3$/ZSM-5, respectively. The stability results of $Ga_2O_3$/ZSM-5 hollow fibers show that the catalytic activity of the catalyst decreases with time on stream, and carbon deposition is the cause of catalyst deactivation since the activity of the $Ga_2O_3$/ZSM-5 hollow fibers was fully recovered after regeneration (Figures S1–S3).

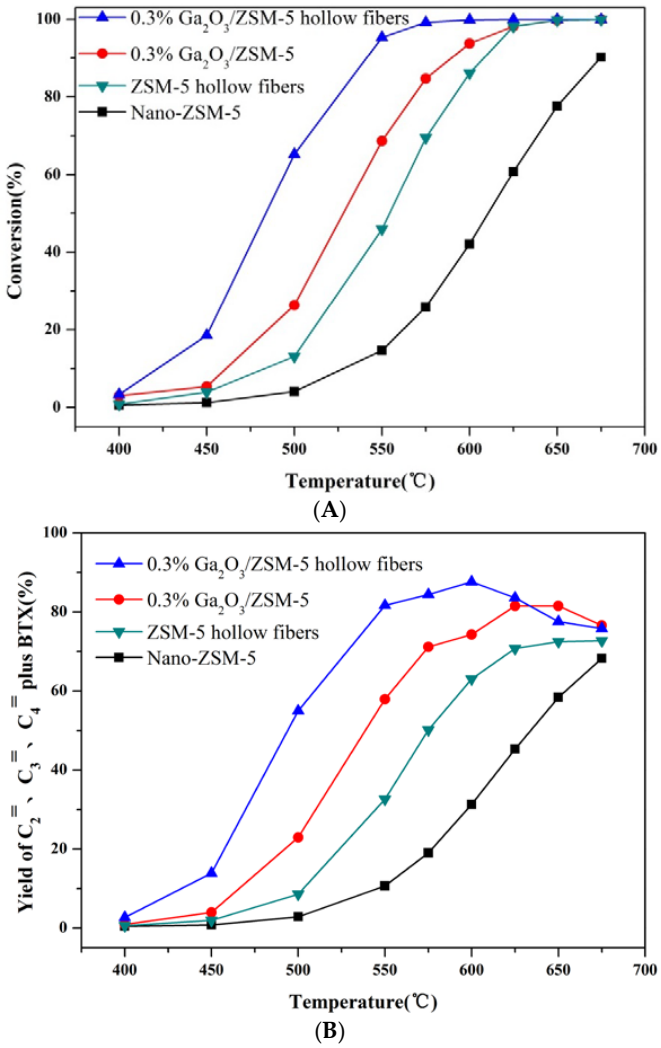


**Figure 8.** The conversion of *n*-butane (A) and the yield of $C_2^=$, $C_3^=$, $C_4^=$ plus BTX (B) as a function of reaction temperatures: 0.3% $Ga_2O_3$/ZSM-5 hollow fibers, 0.3% $Ga_2O_3$/ZSM-5, ZSM-5 hollow fibers, and Nano-ZSM-5.

## 3. Experimental Section

### *3.1. Catalyst Preparation*

#### 3.1.1. ZSM-5 Nanocrystals Preparation

ZSM-5 nanocrystals were prepared by hydrothermal crystallization from a clear solution with the composition of 9TPAOH:0.125$Al_2O_3$:25$SiO_2$:599$H_2O$:1.3NaOH according to previous literature [12,36] except that the addition of NaOH and the synthesis was carried out at 100 °C for 72 h. When the synthesis was completed, the nanocrystals products were washed, dried, and calcined at 550 °C for 6 h in muffle furnace followed by ion-exchanged, dried, and calcined process. The zeolite prepared according to the above methods is denoted Nano-ZSM-5 (with an actual Si/Al of 55 determined by XRF).

#### 3.1.2. $Ga_2O_3$/ZSM-5 Preparation

The as-prepared Nano-ZSM-5 was subsequently impregnated by the incipient wetness technique using aqueous solution of $Ga(NO)_3 \cdot xH_2O$, dried for 10 h at 100 °C, and calcined at 600 °C for 6 h. Catalysts prepared in this way with $x$ wt. % of $Ga_2O_3$ are denoted $x$% $Ga_2O_3$/ZSM-5.

#### 3.1.3. Hierarchical $Ga_2O_3$/ZSM-5 Hollow Fibers Preparation

The outer fluid was prepared as follows: 1.5 g dry $Ga_2O_3$/ZSM-5 nanocrystals were added to 12.16 g absolute ethanol in a beaker (sealed by plastic wrap) and the mixture was subjected to ultrasonic treatment at 100 W for 8 h in order to the nanocrystals be fully dispersed in absolute ethanol. Then, 2.5 g PVP powder was added into the suspension followed by stirring to dissolve PVP powder completely. At last, in order to exclude bubbles in the suspension, another 0.5 h sonication treatment was conducted.

The electrospinning experimental device and the process of electrospinning are similar to that described in the literature [12] except that the flow rate of the paraffin oil is 0.8 mL$\cdot$ h$^{-1}$. The as-prepared fibers are denoted $x$% $Ga_2O_3$/ZSM-5 hollow fibers.

### *3.2. Catalyst Characterization*

X-ray powder diffraction (XRD) patterns in the range of 5°–50° were recorded on a powder X-ray diffractometer(Shimadzu XRD 6000) (Shimadzu, Tokyo, Japan) using CuK$\alpha$ radiation ($\lambda$ = 0.15406 nm) with a scanning rate of 2°/min, voltage 40 kV, and current 30 mA. Quanta 200F (FEI, Hillsboro, OR, USA) scanning electron microscpy (SEM) was used to observe morphology of the catalysts, and it was also employed for EDX line scan. TEM images were obtained by a JEOL JEM 2100 electron microscope (JEOL, Tokyo, Japan) equipped with a field emission source at an accelerating voltage of 200 kV. The BET specific surface area and pore volume of the samples were determined by adsorption-desorption of nitrogen at liquid nitrogen temperature, using a Micromeritics TriStar II 3020 porosimetry analyzer (Micromeritics, Norcross, GA, USA). X-ray photoelectron spectroscopy (XPS) was applied to analyze the change of surface composition performed on a PerkinElmer PHI-1600 ESCA (PerkinElmer, Waltham, MA, USA) spectrometer using Mg$\cdot$ Ka (hv = 1253.6 eV, 1 eV = 1.603 $\times$ $10^{-19}$ J) X-ray source. The binding energy values were corrected for charging effect by referring to the adventitious C1s line at 284.6 eV.

Acidic properties of the catalysts were characterized by the temperature-programmed desorption of ammonia ($NH_3$-TPD) method. 0.1 g sample was pretreated in nitrogen at 600 °C for 1 h, cooled to room temperature, and adsorbed $NH_3$ for 30 min. After flushing with pure nitrogen gas for 45 min, TPD started at a rate of 10 °C/min from 100 °C to 600 °C and the signal was monitored with a thermal conductivity detector (TCD). The TG-DSC test was performed to analyze the amount of carbon deposition using METTLER TOLEDO TGA/DSC 1 (Mettler Toledo, Zurich, Switzerland), at a heating rate of 10 °C/min from 30 °C to 800 °C in an oxygen atmosphere.

### *3.3. Reaction Testing*

Catalytic tests were performed in a fixed-bed flow reactor by passing a gaseous of *n*-butane (2 mL·min$^{-1}$, 99.9%) in nitrogen at a flow rate of 38 mL/min, and the catalyst load was 200 mg. The products were analyzed on-line using a gas chromatograph (SP-2100) (Beifen-Ruili, Beijing, China) equipped with a 30 m GS-ALUMINA capillary column and a FID detector (Beifen-Ruili, Beijing, China), and the contents of them are calculated on hydrocarbon basis (Tables S2–S7).

## 4. Conclusions

The dehydrogenation component of $Ga_2O_3$ was introduced to acid-based ZSM-5 nanocrystals, using $Ga_2O_3$/ZSM-5 nanoparticles as building blocks, $Ga_2O_3$/ZSM-5 hollow fibers with hierarchical macro-meso-microporosity were successfuly prepared by coaxial electrospinning. High conversion activity of *n*-butane and good yield of $C_2^=$, $C_3^=$, $C_4^=$ plus BTX were demonstrated. Superior catalytic performances are attributed to the good banlance of the cracking function of ZSM-5 and the dehydrogenation of $Ga_2O_3$, and the synergetic effect of bifunctionality and hierarchical porosity. The present results help to cast new light on the design of bifunctional fiber-based catalysts for efficient catalytic conversion of light alkanes.

**Acknowledgments:** The authors thank the support of this work by the National Basic Research Program of China (973 Program, No. 2012CB215001), National Science Foundation of China (Grant No. U1162117), Beijing Higher Education Young Elite Teacher Project (YETP0696), and Prospect Oriented Foundation of China University of Petroleum, Beijing (Grant No. ZX20140257).

**Author Contributions:** J.H., S.H., J.L., Y.Z., Y.L., and R.W. performed the experiments and conducted the catalytic activity tests. J.H., G.J., and Z.Z. conceived and designed the experiments, analyzed the experimental data, and wrote the paper. C.X., Y.W., A.D., J.L. and Y.W. interpreted the results, and gave advice about the data analysis as well as the preparation of the manuscript.

**Conflicts of Interest:** The authors declare no conflict of interest.

## References

1. Maia, A.J.; Oliveira, B.G.; Esteves, P.M.; Louis, B.; Lam, Y.L.; Pereira, M.M. Isobutane and *n*-butane cracking on Ni-ZSM-5 catalyst: Effect on light olefin formation. *Appl. Catal. A* **2011**, *403*, 58–64. [CrossRef]
2. Meng, X.; Wang, Z.; Zhang, R.; Xu, C.; Liu, Z.; Wang, Y.; Guo, Q. Catalytic conversion of C4 fraction for the production of light olefins and aromatics. *Fuel Process. Technol.* **2013**, *116*, 217–221. [CrossRef]
3. Rahimi, N.; Karimzadeh, R. Catalytic cracking of hydrocarbons over modified ZSM-5 zeolites to produce light olefins: A review. *Appl. Catal. A* **2011**, *398*, 1–17. [CrossRef]
4. Pollesel, P.; Bellussi, G. Industrial applications of zeolite catalysis: Production and uses of light olefins. *Stud. Surf. Sci. Catal.* **2005**, *158*, 1201–1212.
5. Janda, A.; Bell, A.T. Effects of Si/Al ratio on the distribution of framework Al and on the rates of alkane monomolecular cracking and dehydrogenation in H-MFI. *J. Am. Chem. Soc.* **2013**, *135*, 19193–19207. [CrossRef] [PubMed]
6. Lin, L.; Qiu, C.; Zhuo, Z.; Zhang, D.; Zhao, S.; Wu, H.; Liu, Y.; He, M. Acid strength controlled reaction pathways for the catalytic cracking of 1-butene to propene over ZSM-5. *J. Catal.* **2014**, *309*, 136–145. [CrossRef]
7. Wang, Y.; Yokoi, T.; Namba, S.; Kondo, J.N.; Tatsumi, T. Catalytic cracking of *n*-hexane for producing propylene on MCM-22 zeolites. *Appl. Catal. A* **2015**, *504*, 192–202. [CrossRef]
8. Pant, K.K.; Kumar, V.A.; Kunzru, D. Potassium-containing calcium aluminate catalysts for pyrolysis of *n*-heptane. *Appl. Catal. A* **1997**, *162*, 193–200.
9. Jeong, S.M.; Chae, J.H.; Lee, W.-H. Study on the Catalytic Pyrolysis of Naphtha over a $KVO_3/\alpha$-$Al_2O_3$ Catalyst for Production of Light Olefins. *Ind. Eng. Chem. Res.* **2001**, *40*, 6081–6086. [CrossRef]
10. Al-Yassir, N.; Le van Mao, R.; Heng, F. Cerium promoted and silica-alumina supported molybdenum oxide in the zeolite-containing hybrid catalyst for the selective deep catalytic cracking of petroleum naphthas. *Catal. Lett.* **2005**, *100*, 1–6. [CrossRef]

11. Na, J.; Liu, G.; Zhou, T.; Ding, G.; Hu, S.; Wang, L. Synthesis and Catalytic Performance of ZSM-5/MCM-41 Zeolites With Varying Mesopore Size by Surfactant-Directed Recrystallization. *Catal. Lett.* **2013**, *143*, 267–275. [CrossRef]
12. Liu, J.; Jiang, G.; Liu, Y.; Di, J.; Wang, Y.; Zhao, Z.; Sun, Q.; Xu, C.; Gao, J.; Duan, A.; *et al*. Hierarchical macro-meso-microporous ZSM-5 zeolite hollow fibers with highly efficient catalytic cracking capability. *Sci. Rep.* **2014**. [CrossRef] [PubMed]
13. Wan, J.; Wei, Y.; Liu, Z.; Li, B.; Qi, Y.; Li, M.; Xie, P.; Meng, S.; He, Y.; Chang, F. A ZSM-5-based Catalyst for Efficient Production of Light Olefins and Aromatics from Fluidized-bed Naphtha Catalytic Cracking. *Catal. Lett.* **2008**, *124*, 150–156. [CrossRef]
14. Zhao, G.; Teng, J.; Xie, Z.; Jin, W.; Yang, W.; Chen, Q.; Tang, Y. Effect of phosphorus on HZSM-5 catalyst for C4-olefin cracking reactions to produce propylene. *J. Catal.* **2007**, *248*, 29–37. [CrossRef]
15. Wakui, K.; Satoh, K.; Sawada, G.; Shiozawa, K.; Matano, K.; Suzuki, K.; Hayakawa, T.; Yoshimura, Y.; Murata, K.; Mizukami, F. Dehydrogenation cracking of *n*-butane over modified HZSM-5 catalysts. *Catal. Lett.* **2002**, *81*, 83–88. [CrossRef]
16. Lu, J.; Zhao, Z.; Xu, C.; Zhang, P.; Duan, A. FeHZSM-5 molecular sieves-Highly active catalysts for catalytic cracking of isobutane to produce ethylene and propylene. *Catal. Commun.* **2006**, *7*, 199–203. [CrossRef]
17. Wang, X.; Zhao, Z.; Xu, C.; Duan, A.; Zhang, L.; Jiang, G. Effects of Light Rare Earth on Acidity and Catalytic Performance of HZSM-5 Zeolite for Catalytic Cracking of Butane to Light Olefins. *J. Rare Earths* **2007**, *25*, 321–328.
18. Jiang, G.; Zhang, L.; Zhao, Z.; Zhou, X.; Duan, A.; Xu, C.; Gao, J. Highly effective P-modified HZSM-5 catalyst for the cracking of C4 alkanes to produce light olefins. *Appl. Catal. A* **2008**, *340*, 176–182. [CrossRef]
19. Jia, C.-J.; Liu, Y.; Schmidt, W.; Lu, A.-H.; Schüth, F. Small-sized HZSM-5 zeolite as highly active catalyst for gas phase dehydration of glycerol to acrolein. *J. Catal.* **2010**, *269*, 71–79. [CrossRef]
20. Zhao, L.; Shen, B.; Gao, J.; Xu, C. Investigation on the mechanism of diffusion in mesopore structured ZSM-5 and improved heavy oil conversion. *J. Catal.* **2008**, *258*, 228–234. [CrossRef]
21. Choi, M.; Na, K.; Kim, J.; Sakamoto, Y.; Terasaki, O.; Ryoo, R. Stable single-unit-cell nanosheets of zeolite MFI as active and long-lived catalysts. *Nature* **2009**, *461*, 246–249. [CrossRef] [PubMed]
22. Martens, J.A.; Blomsma, E.; Jacobs, P.A. Isomerization and Hydrocracking of Heptane over Bimetallic Bifunctional PtPd/H-Beta and PtPd/USY Zeolite Catalysts. *J. Catal.* **1997**, *165*, 241–248.
23. Kim, J.; Kim, W.; Seo, Y.; Kim, J.-C.; Ryoo, R. *n*-Heptane hydroisomerization over Pt/MFI zeolite nanosheets: Effects of zeolite crystal thickness and platinum location. *J. Catal.* **2013**, *301*, 187–197. [CrossRef]
24. Jackson, S.; Rugmini, S. Dehydrogenation of *n*-butane over vanadia catalysts supported on θ-alumina. *J. Catal.* **2007**, *251*, 59–68. [CrossRef]
25. Vanlingen, J.; Gijzeman, O.; Weckhuysen, B.; Vanlenthe, J. On the umbrella model for supported vanadium oxide catalysts. *J. Catal.* **2006**, *239*, 34–41. [CrossRef]
26. Cabrera, F.; Ardissone, D.; Gorriz, O.F. Dehydrogenation of propane on chromia/alumina catalysts promoted by tin. *Catal. Today* **2008**, *133–135*, 800–804. [CrossRef]
27. Santhoshkumar, M.; Hammer, N.; Ronning, M.; Holmen, A.; Chen, D.; Walmsley, J.; Oye, G. The nature of active chromium species in Cr-catalysts for dehydrogenation of propane: New insights by a comprehensive spectroscopic study. *J. Catal.* **2009**, *261*, 116–128. [CrossRef]
28. Karamullaoglu, G.; Onen, S.; Dogu, T. Oxidative dehydrogenation of ethane and isobutane with chromium-vanadium-niobium mixed oxide catalys. *Chem. Eng. Process.* **2002**, *41*, 337–347.
29. Nakagawa, K.; Okamura, M.; Ikenaga, N.; Suzuki, N.; Kobayashi, T. Dehydrogenation of ethane over gallium oxide in the presence of carbon dioxide. *Chem. Commun.* **1998**, *9*, 1025–1026. [CrossRef]
30. Sattler, J.J.; Gonzalez-Jimenez, I.D.; Luo, L.; Stears, B.A.; Malek, A.; Barton, D.G.; Kilos, B.A.; Kaminsky, M.P.; Verhoeven, T.W.; Koers, E.J.; *et al*. Platinum-promoted $Ga/Al_2O_3$ as highly active, selective, and stable catalyst for the dehydrogenation of propane. *Angew. Chem. Int. Ed. Engl.* **2014**, *53*, 9251–9256. [CrossRef] [PubMed]
31. Joly, J.F.; Ajot, H.; Merlen, E.; Raatz, F.; Alario, F. Parameters affecting the dispersion of the gallium phase of gallium H-MFI aromatization catalysts. *Appl. Catal. A* **1991**, *79*, 249–263. [CrossRef]
32. Drogone, L.; Moggi, P.; Predieri, G.; Zanoni, R. Niobia and silica-niobia catalysts from sol-gel synthesis: An X-ray photoelectron spectroscopic characterization. *Appl. Surf. Sci.* **2002**, *187*, 82–88. [CrossRef]

33. Sun, Y.; Brown, T.C. Catalytic cracking, dehydrogenation, and aromatization of isobutane over Ga/HZSM-5 and Zn/HZSM-5 at low pressures. *Int. J. Chem. Kinet.* **2002**, *34*, 467–480. [CrossRef]
34. Shin, F.; Tatsuski, Y.; Takayuki, K. Reaction Scheme of Aromatization of Butane over Ga Loaded HZSM-5 Catalyst. *J. Jpn. Petrol. Inst.* **1998**, *41*, 37–44.
35. Qiu, P.; Jack, H.L.; Michael, P.R. Characterization of Ga/ZSM-5 for the catalytic aromatization of dilute ethylene streams. *Catal. Lett.* **1998**, *52*, 37–42. [CrossRef]
36. Mintova, S.; Hölzl, M.; Valtchev, V.; Mihailova, B.; Bouizi, Y.; Bein, T. Closely packed zeolite nanocrystals obtained via transformation of porous amorphous silica. *Chem. Mater.* **2004**, *16*, 5452–5459. [CrossRef]